

# Synthesizing Submicron Polyelectrolyte Capsules to Boost Enzyme Immobilization and Enhance Enzyme-Based Immunoassays

Yanna Shao, Yaofeng Zhou, Nuo Chen, Wenxing Xu, Huan Zhou, Weihua Lai, Xiaolin Huang, Xinran Xiang, Qinghua Ye, Jumei Zhang, Juan Wang, Wolfgang J. Parak, Qingping Wu, and Yu Ding\*



Cite This: *ACS Omega* 2023, 8, 12393–12403



Read Online

ACCESS |



Metrics & More

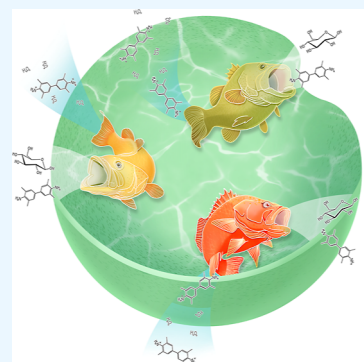


Article Recommendations



Supporting Information

**ABSTRACT:** Polyelectrolyte capsules (PCs) exhibit attractive superiorities in enzyme immobilization, including providing a capacious microenvironment for enzyme conformational freedom, highly effective mass transfer, and protecting enzymes from the external environment. Herein, we provide the first systemic evaluation of submicron PCs (SPCs, 500 nm) for enzyme immobilization. The catalytic kinetics results show that SPC encapsulation affected the affinities of enzymes and substrates but significantly enhanced their catalytic activity. The stability test indicates that SPC-encapsulated horseradish peroxidase (HRP) exhibits ultrahigh resistance to external harsh conditions and has a longer storage life than that of soluble HRP. The proposed encapsulation strategy enables 7.73-, 2.22-, and 11.66-fold relative activities when working at a pH as low as 3, at a NaCl concentration as high as 500 mM, and at a trypsin concentration as high as 10 mg/mL. We find that SPC encapsulation accelerates the cascade reaction efficiency of HRP and glucose oxidase. Owing to SPCs enhancing the catalytic activity of the loaded enzymes, we established an amplified enzyme-linked immunosorbent assay (ELISA) for the detection of *Escherichia coli* O157:H7 using HRP-loaded SPCs. The detection sensitivity of SPC-improved ELISA was found to be 280 times greater than that of conventional HRP-based ELISA. Altogether, we provide an elaborate evaluation of 500 nm SPCs on enzyme immobilization and its application in the ultrasensitive detection of foodborne pathogens. This evaluation provides evidence to reveal the potential advantage of SPCs on enzyme immobilization for enzyme-based immunoassays. It has excellent biological activity and strong stability and broadens the application prospect in urine, soy sauce, sewage, and other special samples.



## 1. INTRODUCTION

Immunoassays are widely used in medicine, agriculture, environmental governance, and bioengineering.<sup>1,2</sup> Among them, enzyme-based immunoassays play a prominent role and are used in commercialized bioanalytical approaches based on the high catalytic activity of commercial enzymes, high selectivity, and mature preparation technology.<sup>3,4</sup> However, it is gradually discovered that conventional enzyme-based immunoassays are limited for trace detection because of their often unsatisfactory detection sensitivity.<sup>5,6</sup> On this basis, a great number of strategies have been developed to improve the detection sensitivity of enzyme-based immunoassays.<sup>7,8</sup> Among them, the utilization of nanomaterials with unique physical and chemical properties to achieve enzyme immobilization is a promising approach in enzyme-based immunoassay research.<sup>9,10</sup> In theory, enzyme immobilization can be used to couple multiple enzyme molecules onto one single nanocarrier to achieve integration of the enzymes' catalytic signals and therefore achieve signal amplification.<sup>11,12</sup> In addition, a great deal of evidence proves that enzyme immobilization can increase the enzymes' half-life, improve their stability, and increase their catalytic activity compared to that of free

enzymes, which can further enhance the detection sensitivity of enzyme-based immunoassays.<sup>13–15</sup>

With the rapid development of nanotechnology, magnetic nanoparticles (NPs),<sup>16</sup> carbon nanotubes,<sup>17</sup> silica-based nanomaterials,<sup>18</sup> cellulose-based nanovesicles,<sup>19</sup> polymer nanocapsules,<sup>20</sup> and resin NPs<sup>21</sup> have been increasingly applied in enzyme engineering because of their favorable properties such as large and unique surface area and special chemical composition. Despite these properties, most confined enzymatic systems are still confronted with great challenges.<sup>22,23</sup> For instance, tightly packed enzymes within host materials typically lack conformational freedom, which may greatly affect molecular recognition.<sup>24</sup> Mass transfer of substrates or products to the enzymes can also be a limiting factor, and thus, internally adsorbed enzymes may display substantially reduced activity.<sup>25</sup> Moreover, traditional incorpo-

Received: January 10, 2023

Accepted: March 10, 2023

Published: March 23, 2023



ration methods, such as adsorption, often result in low loading or high leaching due to weak interaction or pore size mismatching.<sup>26</sup> Therefore, mild immobilization is required, which would ensure maintaining of the enzyme structure, flexible catalytic space to ensure the enzymes' catalytic and conformational freedom, and which would impose only a weak barrier to product or/and substrate mass transfer.

In various enzyme-immobilizing strategies, polyelectrolyte capsules (PCs) have been used for enzyme immobilization due to their simple preparation, stability, adjustable thickness, (in general) biocompatibility, environmental friendliness, and tunable semi-permeability.<sup>27,28</sup> Until now, many natural enzymes, including horseradish peroxidase (HRP),<sup>29</sup> glucose oxidase (GOx),<sup>30</sup> catalase (CAT),<sup>31</sup>  $\alpha$ -galactosidase,<sup>32</sup> alkaline phosphatase,<sup>33</sup> malate dehydrogenase,<sup>34</sup> and so on, have been successfully immobilized in PCs, and these developed biocatalysts have also been broadly used in biosensing, heterogeneous catalysis, clinical medicine, and cell biology. Sufficient research results prove that PCs can encapsulate a large number of different enzyme molecules to achieve enormous signal amplification and can also provide protection for the encapsulated enzyme molecules to extend their storage and catalytic stability.<sup>35,36</sup> Inspired by this, several enzyme-loaded PCs were prepared for establishing improved enzyme-based immunoassays.<sup>37,38</sup> However, most of these enhanced immunoassays still use microscale PCs to encapsulate enzyme molecules. Moreover, there are still few reports focusing on the use of submicron PCs (SPCs) for enzyme immobilization and their applications in enzyme-based immunoassays.

On this basis, we here use 500 nm CaCO<sub>3</sub> NPs, polystyrene sodium sulfonate (PSS), and polyallylamine hydrochloride (PAH) to prepare 500 nm SPCs for investigating the impact of SPCs on enzyme activity and stability in enzyme immobilization. These SPCs are around a factor of 4–10 smaller than typically used PCs with diameters of a few micrometers. The introduction of the porous structure of CaCO<sub>3</sub> NPs as the sacrificial template can provide high loading of enzyme molecules.<sup>39</sup> For investigating the impact of encapsulation by SPCs on the enzymes' activity, we first encapsulated HRP and GOx into the SPCs to prepare HRP@SPCs and GOx@SPCs, respectively. The catalytic kinetic results indicate that the packing into SPCs not only affects the enzymes' affinity to the substrate and their catalytic rate but also may amplify the catalytic signal of the enzymes. Testing of the stability of HRP@SPCs showed that SPCs can provide strong protection for packed HRP under harsh conditions. Subsequently, GOx and HRP were used as a cascade catalysis combination to investigate the potential of SPCs in enzymatic cascade reactions. In this combination, the intermediate product H<sub>2</sub>O<sub>2</sub> was readily consumed by hemin or CAT in biological samples. The results indicate that the microenvironment constructed by SPCs could effectively locally retain H<sub>2</sub>O<sub>2</sub> when CAT was present in the system, thereby maintaining a stable cascade reaction. Based on these results, we then used HRP-loaded SPCs to establish an enzyme-linked immunosorbent assay (ELISA) for the detection of *Escherichia coli* O157:H7. The results show that the detection sensitivity of the enzyme amplification ELISA was 280 times greater than that of the conventional HRP-based ELISA. In general, this work evaluated the potential of 500 nm SPCs as enzyme immobilizers in amplifying enzyme signals, improving enzyme stability, promoting the development of multi-enzyme cascade

reaction catalysts, and enhancing the sensitivity of enzyme-based immunoassays.

## 2. EXPERIMENTAL SECTION

**2.1. Materials.** Calcium chloride (CaCl<sub>2</sub>), sodium carbonate (Na<sub>2</sub>CO<sub>3</sub>), PSS ( $M_w$ : 70,000), PAH ( $M_w$ : 15,000), glycol, bovine serum albumin (BSA), glucose, ethylenediaminetetraacetic acid-2Na (EDTA-2Na), HRP, CAT, and GOx were purchased from Sigma-Aldrich Chemical (Shanghai, China). H<sub>2</sub>O<sub>2</sub>, 3,3',5,5'-tetramethylbenzidine (TMB), streptavidin (SA), sulfo-NHS-biotin, fluorescein isothiocyanate (FITC), and rhodamine B (RhB) isothiocyanate were purchased from Thermo Fisher Scientific Inc. (Shanghai, China). Purified Milli-Q water prepared from the Milli-Q system was used throughout this study (Millipore, Milford, MA, USA). Phosphate buffer (PB, pH 7.4, 0.01 M) was prepared by adding 290.10 mg of Na<sub>2</sub>HPO<sub>4</sub>·12H<sub>2</sub>O and 68.05 mg of NaH<sub>2</sub>PO<sub>4</sub>·2H<sub>2</sub>O in 1000 mL of Milli-Q water. Phosphate-buffered saline (PBS) solution was prepared by adding NaCl into PB at the concentration of 0.01 M. PBST (washing buffer) was prepared by adding 0.5% Tween-20 to the PBS solution. The pH was adjusted to 7.4 before use unless otherwise specified. All other analytical-grade chemicals were purchased from Sinopharm Chemical Corp. (Shanghai, China) and used without further purification.

**2.2. Instrument and Characterization.** UV–visible absorbance spectra were collected using a UV–vis spectrophotometer (G10S, Thermo Fisher Scientific Inc., USA). Dynamic light scattering (DLS) analysis was conducted using a Malvern Nano-Z90 zetasizer (Malvern Panalytical Ltd., Worcestershire, UK). The concentration of SPCs was measured by a NP tracking analysis machine (Nano Sight LM 14C, Malvern Panalytical Ltd.). The shape and size of the NPs were determined with a JEOL transmission electron microscope (JEM 2100, Tokyo, Japan) and a Hitachi scanning electron microscope (S-4800, Tokyo, Japan). A commercial 96-well plate reader was obtained from Corning Inc. Technology Company (Cytation 5, BioTek, USA).

**2.3. Bacterial Culture.** One hundred microliter of the bacterial solution was added to the Luria–Bertani (LB) broth and cultured for 12 h in a 37 °C shaker with noticeable turbidity. The bacteria were activated on the nutrient agar plate and cultured for 12 h in a 37 °C constant-temperature incubator. After colonies appeared, the inoculating loop was used to pick a single colony, inoculate it into the LB broth, and cultivate it overnight in a 37 °C shaker at 150 rpm. One milliliter of the bacterial solution was placed in a 1.5 mL sterile centrifuge tube and gradient diluted with sterile PBS solution (pH 7.4, 0.01 M). Then, 100  $\mu$ L of the diluted bacterial solution was applied to the nutrient agar plate and placed in a 37 °C incubator for counting. The high concentration of the bacterial solution was placed in water, boiled for 10 min, and then centrifuged at 8000g for 5 min. The bacteria were washed 3 times with sterile PBS solution. The precipitate was stored at 4 °C for later use after being resuspended.

**2.4. Synthesis of the Enzyme Containing CaCO<sub>3</sub> NPs.** To synthesize CaCO<sub>3</sub> NPs, a synthesis buffer was first prepared by adding 45 g of glycol into 200 g of freshly prepared Milli-Q water. Subsequently, 50 mg/mL PSS solution, 4 mg/mL enzyme solution, 2 mg/mL Na<sub>2</sub>CO<sub>3</sub> solution, and 2 mg/mL CaCl<sub>2</sub> solution were prepared by dissolving the corresponding chemical powder into the synthesis buffer. Then, 1 mL of CaCl<sub>2</sub> solution, 50  $\mu$ L of

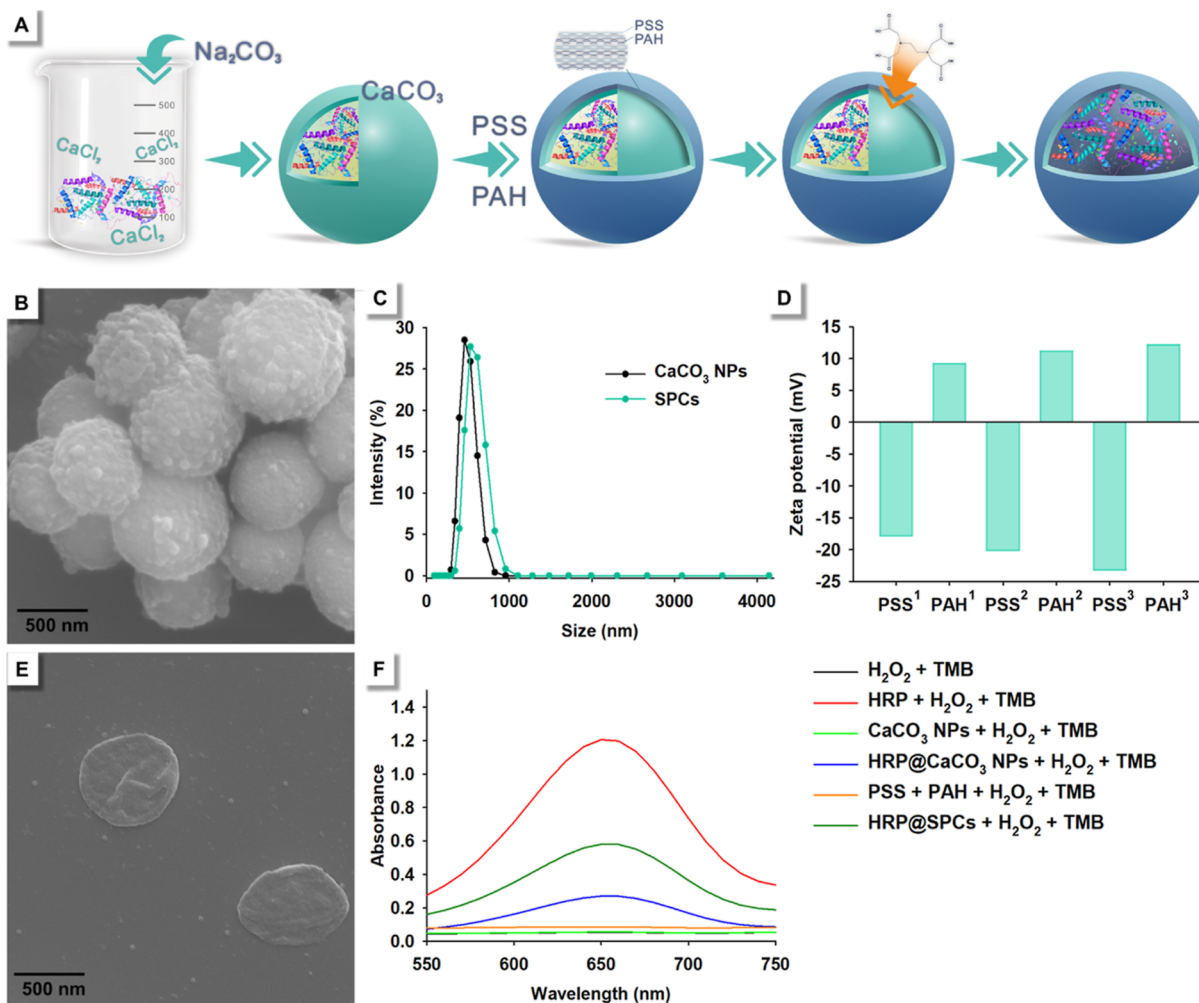


**Figure 1.** Synthesis and characterization of HRP-loaded SPCs (HRP@SPCs). (A) Schematic diagram of the synthesis of enzyme-loaded SPCs. Anion polyelectrolyte PSS was employed to regulate the CaCO<sub>3</sub> synthesis. Then, the prepared CaCO<sub>3</sub> core was coated by PSS and cation polyelectrolyte PAH via layer-by-layer technology. The hollow SPCs were obtained by using EDTA-2Na to dissolve CaCO<sub>3</sub>. (B) SEM image of CaCO<sub>3</sub> NPs. (C) DLS analysis of the hydrodynamic diameter of CaCO<sub>3</sub> NPs and SPCs. (D)  $\zeta$  potentials of the CaCO<sub>3</sub> NPs after the addition of subsequent polyelectrolyte double layers of PSS/PAH. DLS and  $\zeta$  potential analyses were performed in ultrapure water. (E) SEM image of the synthesized HRP@SPCs. (F) UV-vis absorbance spectra of the catalytic reaction of TMB and H<sub>2</sub>O<sub>2</sub> by a series of catalysts.

enzyme solution, and 250  $\mu$ L of PSS solution were added to a 5 mL beaker and stirred at 550 rpm for 10 min to fully form the CaCO<sub>3</sub>@PSS complex. After that, 1 mL of Na<sub>2</sub>CO<sub>3</sub> solution was quickly added into the mixture and stirred at 550 rpm for 30 min. The enzyme containing CaCO<sub>3</sub> NPs with PSS ligand (CaCO<sub>3</sub>@PSS) was purified by centrifugation at 8000g for 10 min, and the precipitate was washed twice with the synthesis buffer.

### 2.5. Synthesis of SPCs with Immobilized Enzymes.

The SPCs were formed by PSS and PAH polyelectrolytes through a layer-by-layer process.<sup>40</sup> The PAH solution was prepared by dissolving PAH powder into the synthesis buffer to a concentration of 30 mg/mL. Next, a layer-by-layer process was carried out on the 500 nm CaCO<sub>3</sub>@PSS containing the enzymes. First, the as-prepared CaCO<sub>3</sub>@PSS was resuspended in 950  $\mu$ L of synthesis buffer, and then 50  $\mu$ L of PAH solution was added to this mixture and ultrasonicated for 5 min. The ultrasonically treated solution was then moved to a shaker and shaken for 15 min. The PAH-coated NPs (CaCO<sub>3</sub>@PSS/PAH) were then purified through centrifugation at 8000g for 10 min. The precipitate was washed twice with the synthesis

buffer. Similar procedures were applied to achieve subsequent additional PSS and PAH layers. Finally, the resulting CaCO<sub>3</sub>@(PSS/PAH)<sub>n</sub> NPs were suspended in 1 mL of Milli-Q water and stored at 4 °C for further use.

Afterward, 5 mL of the freshly prepared EDTA-2Na solution was then added into the above-prepared CaCO<sub>3</sub>@(PSS/PAH)<sub>n</sub> NP solutions to dissolve the CaCO<sub>3</sub> core. These mixtures were then moved to 4 °C and kept dissolving overnight. The capsules were purified by centrifugation at 8000g for 15 min and resuspended in Milli-Q water.

### 2.6. Measurement of the Catalytic Kinetics of Soluble and SPC-Immobilized Enzymes.

Kinetic measurements were carried out by following the enzymatic (i.e., HRP caused) conversion of TMB by monitoring the change in absorbance at 650 nm with 0.5 min intervals.<sup>41</sup> Experiments were conducted using 11 pM HRP in 1.0 mL of 0.10 M sodium acetate (NaAc) buffer (pH 5.0) at 37 °C or 0.125 pM HRP@SPCs in 1.0 mL of 0.10 M NaAc buffer (pH 5.0) at 37 °C. To investigate the double reciprocal plots of the activity of HRP, assays were performed under standard reaction conditions as described above by varying the concentrations

of TMB at a fixed concentration of  $\text{H}_2\text{O}_2$  or vice versa. The Michaelis–Menten constant was calculated using the Lineweaver Burk plot:  $1/V = K_m/(V_{\max}[S]) + 1/V_{\max}$ , where  $V$  is the initial velocity,  $V_{\max}$  is the maximal reaction velocity, and  $[S]$  corresponds to the substrate concentration.<sup>42</sup> As reported by Zhang et al.,<sup>43</sup> the catalytic kinetics of GOx were measured by using a similar procedure via an HRP-coupled colorimetric assay. In brief, GOx was used to catalyze glucose, and the generated  $\text{H}_2\text{O}_2$  could be measured by an HRP-carried out colorimetry assay.

**2.7. Preparation of FITC-Labeled HRP- and RhB-Labeled GOx.** One milliliter of 1 mg/mL FITC solution was mixed with 20 mg/mL HRP solution and 0.13 M  $\text{NaHCO}_3$  solution (pH 8.0) for 12 h to prepare FITC-labeled HRP. Then, the excess FITC was removed using a PD-10 chromatographic column (Global Life Sciences Solutions Operations UK Ltd., 17-0851-01). FITC-labeled HRP was recovered by freeze-drying for further use. RhB-labeled GOx was prepared by a similar procedure.

**2.8. Biotin-Labeling of Detection Antibodies.** Four milligrams of antibodies was added to a sulfo–NHS–biotin solution (0.05 mg/mL) dissolved in PBS solution (pH 7.4, 0.01 M). The reaction was carried out on a mixer for 4 h, followed by dialysis with PBS solution (0.01 M, pH 7.4) for 3 days in order to get purified biotinylated antibodies.

**2.9. SA-Labeled HRP@SPCs.** With reference to the method reported by Shao et al., we directly coupled SA and SPCs through an electrostatic interaction.<sup>44</sup> First, SA was added to 1 mL of SPC solution (PBS, pH 6.5, 0.01 M) dropwise to a final concentration of 10  $\mu\text{g}/\text{mL}$  and was reacted at 25 °C for 60 min. After the reaction, 100  $\mu\text{L}$  of 1% (W/V) BSA solution was added to block the excess sites on the SPCs by a 30 min reaction. Excess BSA and SA were removed by centrifugation and removal of the supernatant containing the free BSA and SA, and the precipitate containing the SA-labeled HRP@SPCs was redissolved in 500  $\mu\text{L}$  of PBS.

**2.10. Detection Procedure of the HRP@SPC-Based ELISA.** First, 100  $\mu\text{L}$  of antibody (5  $\mu\text{g}/\text{mL}$ ) used as the capture antibody for the coating of the plates was dissolved in PBS buffer (0.01 M, pH 7.4), and the solution was added to a 96-well plate and reacted overnight at 4 °C. After the reaction, the plate was washed with PBST 3 times, and 300  $\mu\text{L}$  of BSA (10 mg/mL), used for blocking non-specific adsorption, was added to react at 37 °C for 2 h. Then, the 96-well plate was rewashed with PBST 3 times, and 100  $\mu\text{L}$  of the standard samples to be tested with different concentrations was added and reacted at 37 °C for 1 h. Next, the 96-well plate was washed with PBST 3 times, and 100  $\mu\text{L}$  of biotin-labeled detection antibody (10  $\mu\text{g}/\text{mL}$ ) was added at 37 °C for 1 h. After the reaction, the 96-well plate was washed 3 times by PBST for removing the excess biotinylated detection antibodies. Afterward, 100  $\mu\text{L}$  of SA-SPC (15  $\mu\text{g}/\text{mL}$ ) was added to the microplate, and the 96-well plate was placed at 37 °C to connect HRP-loaded SPCs and the immunocomplex by the highly effective reaction of biotin and SA. Then, the 96-well plate was washed 3 times for removing the unreacted SA-SPCs. Finally, 100  $\mu\text{L}$  of the TMB substrate was added to each well of the plate, and the 96-well plate was placed at 37 °C for 30 min. The absorbance at 650 nm was measured with a 96-well plate reader and photographed with a camera.

### 3. RESULTS AND DISCUSSION

**3.1. Synthesis and Characterization of Enzyme-Loaded Capsules.** In the present work, the classical layer-by-layer technology was used to prepare SPCs by employing  $\text{CaCO}_3$  NPs as the sacrificial template (Figure 1A). HRP-loaded  $\text{CaCO}_3$  NPs (HRP@ $\text{CaCO}_3$  NPs) were first synthesized by a PSS-regulated method. As shown in Figure 1B, the synthesized HRP@ $\text{CaCO}_3$  NPs exhibited uniform sphericity with a diameter of  $530 \pm 57$  nm ( $n = 50$ ). The hydrodynamic diameter of HRP@ $\text{CaCO}_3$  NPs was measured as 497 nm (Figure 1C). Afterward, a polyelectrolyte layer coating was formed by a lay-by-layer assembly process (Figure 1A). In theory, more layers of PSS and PAH can provide higher stability to avoid unwanted leakage.<sup>45</sup> However, as each additional layer requires a washing step, the increased number of washing steps also can lead to a loss of the encapsulated molecules. PSS and PAH layers may also restrict the catalytic activity of the packed enzymes, e.g., due to hindered transport of enzymatic substrates and products. Therefore, we first optimized the layer number of PSS and PAH layers by measuring the relative catalytic activity to obtain high catalytic activity and stability. As shown in Figure S1, the relative catalytic activity and the leakage ratio of HRP-loaded  $\text{CaCO}_3@(\text{PSS}/\text{PAH})_n$  decrease as the number of PSS/PAH layers increases before three PSS/PAH layers. Thus, the optimum layer number of PSS/PAH was found to be 3. The results of  $\zeta$ -potential measurements for each layer indicated that PSS and PAH were successfully coated on the surface of  $\text{CaCO}_3$  NPs (Figure 1D). Figure 1C shows a slight increase in size after dissolving the  $\text{CaCO}_3$  template cores. Subsequently, the saturated HRP loading amount was optimized. In the optimization, 0, 0.25, 0.50, 1.00, 2.00, and 4.00 mg/mL HRP solutions were used to synthesize  $\text{CaCO}_3@(\text{PSS}/\text{PAH})_3$ . Figure S2 shows that the absorbance value gradually increases with the increase of HRP concentration and then begins to stabilize when the HRP concentration is 1 mg/mL, indicating the saturation effect. Under the same  $\text{CaCO}_3@(\text{PSS}/\text{PAH})_3$  concentration,  $\text{CaCO}_3@(\text{PSS}/\text{PAH})_3$  prepared by 1 mg/mL HRP solution had the highest catalytic activity. Hence, 1 mg/mL HRP was used to prepare the HRP-loaded  $\text{CaCO}_3@(\text{PSS}/\text{PAH})_3$ . After preparing HRP-loaded  $\text{CaCO}_3@(\text{PSS}/\text{PAH})_3$ , the  $\text{CaCO}_3$  template was dissolved by EDTA-2Na to prepare HRP-loaded SPCs (HRP@SPCs). A complete and hollow structure of HRP@SPCs is presented in the SEM image (Figure 1E). Catalytic properties of the HRP@SPCs were tested by catalyzing  $\text{H}_2\text{O}_2$  and TMB. As shown in Figure S3, HRP@ $\text{CaCO}_3$  NP- and HRP@SPC-catalyzed  $\text{H}_2\text{O}_2$  and TMB exhibited the typical blue color. The relevant UV absorbance spectrum (Figure 1F) showed that the maximum absorbance of the blue solution is 650 nm. All the above results confirmed that HRP was successfully loaded into the HRP@SPCs.

**3.2. Catalytic Kinetics of Soluble and SPC-Packed HRP.** After preparing the HRP@SPCs, the impact of SPCs on the catalytic kinetics of HRP was evaluated by a steady-state kinetics assay. By comparing the catalytic kinetics of HRP and HRP@SPCs, the signal amplification potential of SPC-based HRP immobilization and the effect of packing HRP into SPCs can be roughly understood. Before the evaluation, the catalytic conditions of HRP and HRP@SPCs, including reaction temperature,  $\text{H}_2\text{O}_2$  concentration, pH, and reaction time, were optimized. Figure S4 shows that the optimum catalytic conditions of HRP@SPCs are 37 °C, 0.1 M  $\text{H}_2\text{O}_2$ , pH 5.0, and

Table 1. Catalytic Kinetics of HRP, GOx, HRP@SPCs, and GOx@SPCs according to the Michaelis–Menten Model<sup>a</sup>

E = enzyme	[E] (M)	substrate	$K_m$ (mM)	$V_{max}$ ( $10^{-8}$ M/s)	$K_{cat}$ ( $s^{-1}$ )
HRP	$1.10 \times 10^{-11}$	H <sub>2</sub> O <sub>2</sub>	2.39	3.21	$2.92 \times 10$
HRP	$1.10 \times 10^{-11}$	TMB	0.26	4.61	$4.18 \times 10^3$
HRP@SPCs	$1.25 \times 10^{-13}$	H <sub>2</sub> O <sub>2</sub>	51.80	1.15	$9.20 \times 10^4$
HRP@SPCs	$1.25 \times 10^{-13}$	TMB	0.20	0.71	$5.68 \times 10^4$
GOx	$5.00 \times 10^{-10}$	glucose	4.23	253.66	$5.07 \times 10^3$
GOx@SPCs	$1.00 \times 10^{-11}$	glucose	54.94	357.50	$3.58 \times 10^5$

<sup>a</sup>The concentrations of HRP, GOx, HRP@SPCs, and GOx@SPCs were 11 pM, 0.125 pM, 0.5 nM, and 1 nM, respectively.

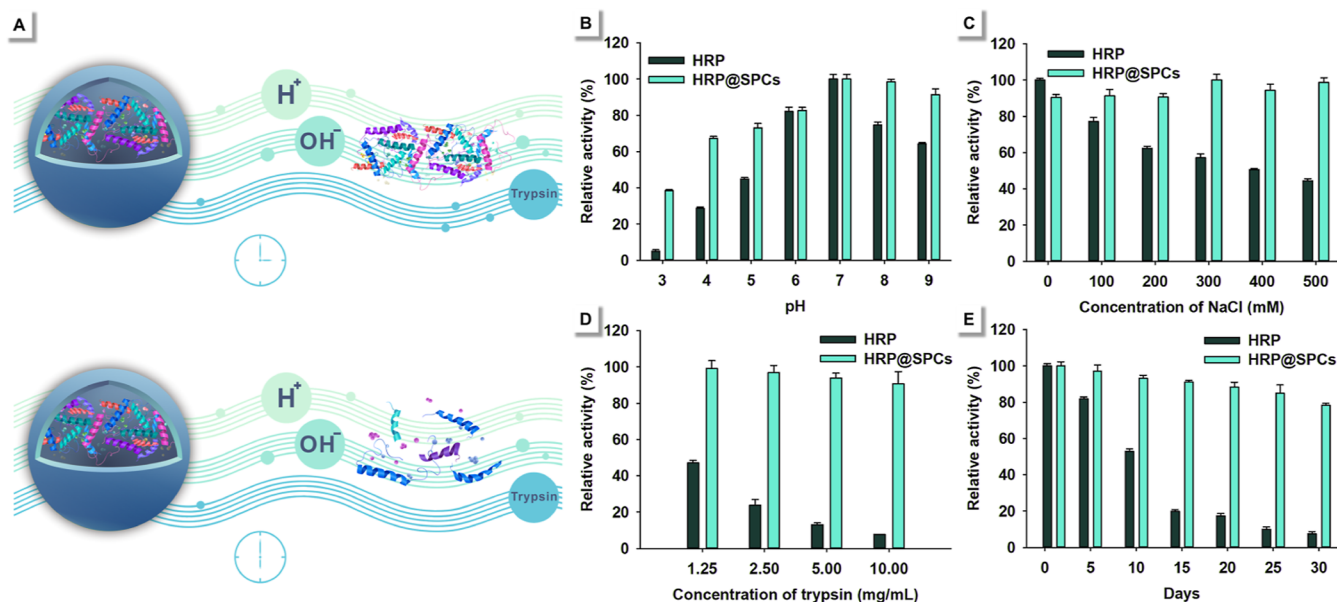


**Figure 2.** Evaluation of the stability of HRP@SPCs and free HRP. (A) Scheme of SPCs on the protection of the encapsulated enzyme. Under the protection of SPCs, the immobilized enzyme shows higher harsh condition tolerance than the soluble enzyme. (B) Catalytic activity of HRP@SPCs and free HRP after incubation in different pH soluble solutions for 1 h. (C) Effect of NaCl concentration on the activity of HRP@SPCs and soluble HRP. (D) Relative activity of HRP@SPCs and free HRP after exposure to protease trypsin. (E) Storage stability of HRP@SPCs and free HRP at 25 °C and pH 7.0 for 1 month. For each curve, the value for the maximal absorbance at 650 nm was set as 100% of the relative activity. The relative activities of HRP@SPCs and HRP under different conditions were calculated according to the value of 100% of relative activity. All the error bars were calculated by three repetitions.

30 min of catalytic reaction time; the optimum catalytic conditions of soluble HRP were 37 °C, 0.025 M of H<sub>2</sub>O<sub>2</sub>, pH 5.6, and 15 min of catalytic reaction time. After obtaining the optimum catalytic conditions, the parameters involving the Michaelis constant ( $K_m$ ), maximal rate ( $V_{max}$ ), and turnover number ( $K_{cat}$ ) of HRP and HRP@SPCs were measured. Typical Michaelis–Menten equations were obtained by changing the H<sub>2</sub>O<sub>2</sub> or TMB concentrations (Figure S5), and the results are summarized in Table 1. As shown in Table 1, regardless of whether H<sub>2</sub>O<sub>2</sub> or TMB was used as a substrate, the  $K_{cat}$  value of HRP@SPCs showed 1 order of magnitude enhancement compared to that of soluble HRP, indicating that SPC encapsulation is a potential signal amplification strategy for immunoassays.

In contrast, the  $V_{max}$  value and affinity of the enzyme toward the substrate were weakened by SPC encapsulation. Of note, SPC encapsulation exhibited a weaker influence when using TMB as the substrate. These results indicate that SPC encapsulation might impact the enzyme kinetics. To further prove this conclusion, we then used SPCs to load GOx (GOx@SPCs) and tested the catalytic kinetics of soluble GOx and GOx@SPCs using glucose as the substrate (Figure S6). The results in Table 1 show that SPC encapsulation weakens

the affinity of GOx and glucose but promotes the catalytic activity of GOx. Thus, in general, SPC encapsulation reduced the affinity of the enzyme and substrate. This result is probably due to the polyelectrolyte walls that hinder the mass transport of substrates and products. However, concerning catalytic rates, SPC encapsulation exhibited different effectiveness for HRP and GOx. This may explain the current debate about the effect of polyelectrolytes on enzyme activity.<sup>46</sup> The inconsistency in previous reports suggests that the influence of polyelectrolytes on enzyme activity is likely to vary depending on the nature of enzymes and substrates.

**3.3. Protection Performance of SPCs to HRP.** In addition to using SPCs to amplify the catalytic signal to enhance the detection sensitivity of enzyme-based immunoassays, the protection performance of SPCs to the loaded enzyme would also be essential for reducing transportation and storage costs. Herein, we used HRP@SPCs to investigate the environmental tolerance of SPC-packed and soluble HRP through 1 h of treatment under different pH values, NaCl solutions, and trypsin solutions (Figure 2A). The relative catalytic activities of packed HRP and free HRP were monitored through catalytic oxidation of TMB by H<sub>2</sub>O<sub>2</sub>. As shown in Figure 2B, soluble HRP exhibited a lower endurance

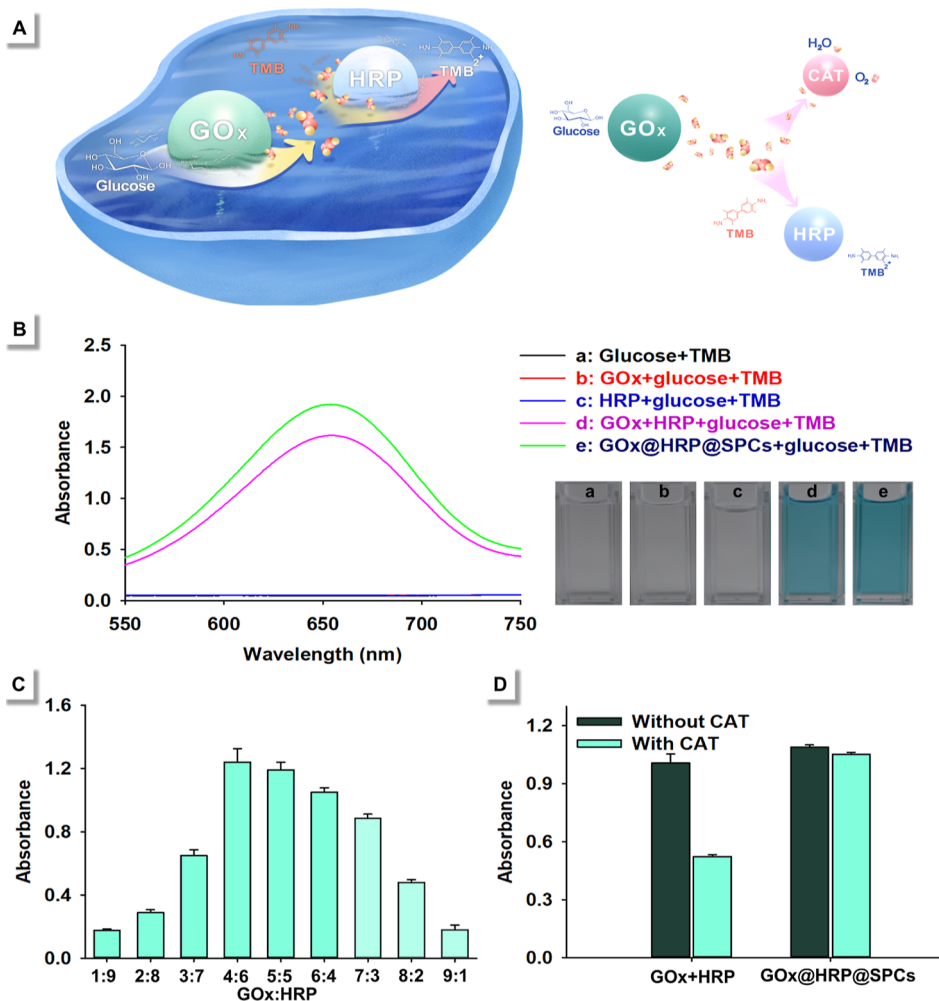


**Figure 3.** SPC-mediated cascade catalytic reaction. (A) Schematic diagram of the GOx@HRP@SPC-based cascade catalytic reaction. In theory, SPC encapsulation enhances the cascade catalytic reaction through promoting present  $\text{H}_2\text{O}_2$  (GOx catalyzes glucose to generate  $\text{H}_2\text{O}_2$ ) to HRP and protecting the degradation of  $\text{H}_2\text{O}_2$  by external CAT. (B) GOx, HRP, GOx plus HRP mixture, and GOx@HRP@SPCs catalyzed glucose and TMB, respectively. The inset is a photograph of these catalytic reactions. (C) Optimization of the ratio of GOx and HRP in synthesizing GOx@HRP@SPCs. (D) Effect of CAT participation on the activity of the GOx plus HRP mixture and the GOx@HRP@SPC cascade system. All the error bars were calculated by three repetitions.

capacity in alkaline and acidic conditions than packed HRP. Meanwhile, packed HRP gave strong endurance capacity in high concentrations of salt solution, which means that SPCs can provide preservation of the loaded HRP (Figure 2C).

On the other hand, soluble HRP lost its catalytic activity at a 10 mg/mL trypsin concentration. In contrast, the catalytic activity of packed HRP had no noticeable change after treatment with high concentrations of trypsin (Figure 2D). All these results proved that SPCs can increase the environmental tolerance of packed HRP. Furthermore, the storage stability of HRP@SPCs was further evaluated by monitoring the catalytic activity of HRP@SPCs and HRP every 5 days. The HRP and HRP@SPCs were dissolved in 0.01 M PBS solution and stored at 25 °C. As shown in Figure 2E, the catalytic activity of soluble HRP had a significant feebleness on the fifth day and left only approximately 10% catalytic activity after 30 days, whereas HRP@SPCs retained almost 80% catalytic activity after being stored at 25 °C for 30 days. This finding indicated the excellent long-term storage stability and absence of significant leakage in HRP@SPCs during storage. Thus, SPCs can provide favorable protection to the loaded HRP. These results generally imply that SPC-based enzyme

amplification has potential for commercial enzyme-based immunoassays, including improved detection sensitivity and reduced transportation and storage costs.

**3.4. SPC-Based Enzyme Cascade Catalysis.** To date, growing cascade biocatalysts have been developed. However, most of these cascade biocatalysts fail in practical applications because the complicated catalytic environment is always unamiable for intermediate products of cascade catalysis.<sup>47</sup> For example, GOx and HRP cascade catalysis-based immunoassays for detecting human blood and living cell samples should consider that GOx-generated  $\text{H}_2\text{O}_2$  may be consumed by hemin or CAT enzymes in the biological environment.<sup>48</sup> However, if cascade catalysis can be completed in an independent microenvironment, the risk of intermediate product consumption could be minimized. Therefore, we hypothesized that SPC-based enzyme cascade catalysis amplification can circumvent this risk because the coloaded enzymes can complete cascade catalysis in SPC-provided microenvironments. To verify this hypothesis, GOx and HRP were chosen as a model cascade combination to synthesize GOx- and HRP-coloaded SPCs (GOx@HRP@SPCs). As shown in Figure 3A, GOx could catalyze glucose to generate

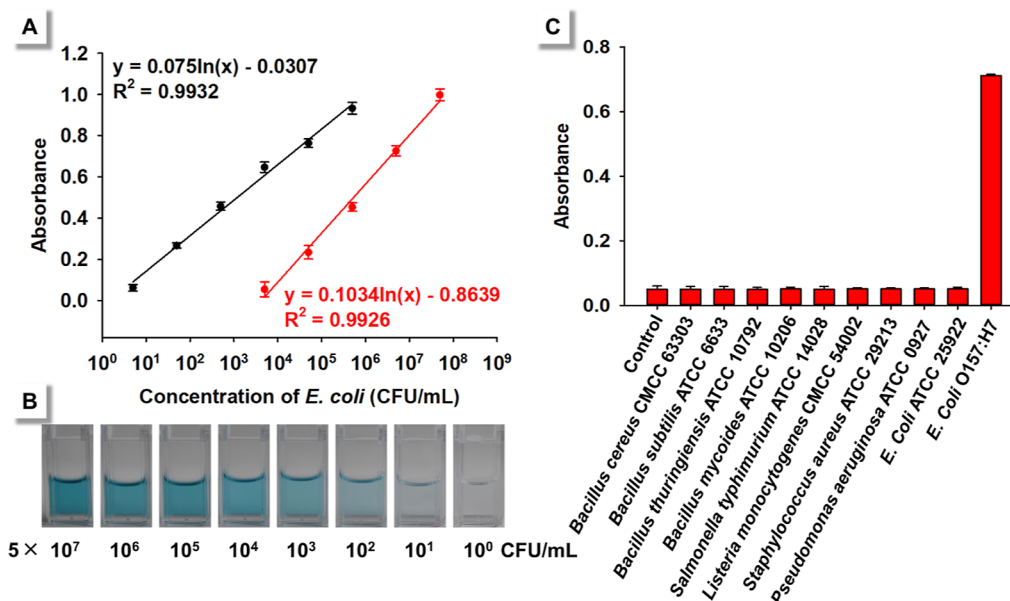


**Figure 4.** Performance of the SPC-based ELISA system on the detection of *E. coli* O157:H7. (A) Calibration curves of HRP-based conventional ELISA (red line) and the proposed SPC-based ELISA (black line). (B) Photographs of the proposed HRP@PC-based ELISA in the spiked PBS solution (0.01 M, pH 7.4) with different concentrations of *E. coli* O157:H7 ( $5 \times 10^0$  to  $5 \times 10^7$  cfu/mL). (C) Specificity of the proposed HRP@PC-based ELISA for other nontarget bacteria ( $1 \times 10^7$  cfu/mL). Each value represents the mean of three independent experiments ( $n = 3$ ). A negative control test was performed by adding a sterile PBS solution. The optical density of the reaction solution after 30 min of incubation was recorded at 650 nm.

gluconic acid and  $H_2O_2$ , which in turn is the substrate for the HRP-catalyzed oxidation of TMB. We used SPCs to encapsulate FITC-labeled HRP and RhB-labeled GOx to verify that GOx and HRP could be loaded into SPCs simultaneously. As shown in Figure S7, the synthesized GOx- and HRP-coloated SPCs (GOx@HRP@SPCs) exhibited a uniform spherical shape with green (FITC) and red (RhB) fluorescence. Then, the catalytic activity of the prepared GOx@HRP@SPCs was evaluated by catalyzing a 250 mM glucose and 8 mM TMB mixture. Interestingly, only GOx@HRP@SPCs and simultaneous addition of GOx and HRP to glucose and TMB could catalyze the oxidation reaction of TMB (Figure 3B). Thus, GOx and HRP were successfully loaded into SPCs and exhibited their intrinsic catalytic activity. We then optimized the ratio of GOx and HRP in SPCs to ensure that the GOx@HRP@SPCs could exhibit the highest catalytic performance. The results in Figure 3C indicate that the optimum ratio of GOx and HRP in synthesizing GOx@HRP@SPCs was GOx/HRP = 4:6. We, however, want to point out that this is the enzyme ratio in the protein mix used for the encapsulation. As the encapsulation efficiency of GOx and HRP could be different, the resulting enzyme ratio in the SPCs could be somewhat different. Under the optimized synthesis conditions, the catalytic conditions, including pH, catalytic temperature, concentration of glucose, catalytic time of GOx@HRP@SPCs, and GOx and HRP combinations, were optimized (Figure S8). In our concept, GOx- and HRP-based cascade catalysis is confined in the SPC-protected microenvironment. The prepared GOx@HRP@SPCs were used to catalyze glucose and TMB mixtures in the presence of CAT to explore this concept. This well-known native enzyme can catalyze the breakdown of  $H_2O_2$  to generate  $O_2$  and  $H_2O$ , protecting cells from the oxidative damage caused by  $H_2O_2$ .<sup>49</sup> For comparison, GOx and HRP combinations with the same enzyme ratio (GOx/HRP =

4:6) and the same concentration of CAT were used. The results in Figure 3D demonstrate that the relative cascade catalysis efficiency of GOx@HRP@SPCs was maintained at 95% after adding CAT into the reaction. In contrast, the GOx and HRP combination (i.e., the enzymes without encapsulation) retained only 48% cascade catalysis efficiency upon the addition of CAT. These results prove that SPCs can provide an independent microenvironment for cascade catalysis and therefore assist cascade catalysis-based immunoassays in circumventing disturbance from samples.

**3.5. Development of HRP@SPC-Based ELISA for Ultrasensitive Detection of *E. coli* O157:H7.** ELISA is one of the most common immunoassays for detecting biochemical targets and has been widely used in food safety, environmental monitoring, and clinical diagnosis.<sup>50</sup> Nevertheless, the major drawback of conventional ELISA is the relatively low detection sensitivity when using HRP to label biorecognition molecules (e.g., antibodies and aptamers).<sup>5</sup> Therefore, enzyme-based amplification technology is a promising strategy to increase the detection sensitivity of ELISA.<sup>4</sup> Herein, we established an HRP@SPC-based ELISA to test SPC-based enzyme amplification for performing signal amplification in immunoassays. In this ELISA, *E. coli* O157:H7 was chosen as the model target analyte because *E. coli* O157:H7 is a common pathogenic bacterium and requires a very low detection rate or no detection in the food safety standards of many countries.<sup>51</sup> As shown in Figure S9, the designed capsule-based strategy for the fabrication of highly efficient biocatalysts was then integrated into the ELISA platform with the help of a biotin–SA system to realize highly sensitive detection of *E. coli* O157:H7. In brief, *E. coli* O157:H7 in the sample solution bound to the capture antibodies that were immobilized on 96-well plates, to form immunocomplexes. The formed complexes could then capture biotinylated detection antibodies, and then the captured

biotinylated detection antibodies were further linked to SA-labeled HRP@SPCs for detection. To gain the highest detection sensitivity, the coupling conditions of pH and the content of SA on the surface of the SPCs were optimized (Figure S10). Then, the detection conditions also were optimized by a checkerboard titration method at an *E. coli* O157:H7 concentration of  $1 \times 10^5$  cfu/mL. Table S1 shows that the optimal concentrations of biotinylated detection antibodies and capture antibodies were 1.25 and 5  $\mu\text{g/mL}$ , respectively. As a comparison, a conventional ELISA was established by a similar method.

Under these optimized conditions, standard curves of HRP@SPCs and HRP-based ELISA for detecting *E. coli* O157:H7 were generated by analyzing a series of *E. coli* O157:H7-spiked milk standard solutions. Using conventional HRP-based ELISA, the standard curve showed a linear detection range at *E. coli* O157:H7 concentrations from  $5 \times 10^4$  to  $5 \times 10^7$  cfu/mL, with a correlation coefficient ( $R^2 = 0.9926$ ; Figure 4A). After SPC amplification, the linear detection range of HRP@SPC-based ELISA was  $5 \times 10^1$  to  $5 \times 10^5$  cfu/mL ( $R^2 = 0.9932$ ; Figure 4A). Even at  $5 \times 10^1$  cfu/mL, the wells also exhibited a distinctive blue color, whereas no color changes appeared in the negative control well (Figure 4B). This result demonstrates the potential of the HRP@SPC-based ELISA in detecting ultralow concentrations of *E. coli* O157:H7, including a single bacterial cell in a 100  $\mu\text{L}$  sample solution. Conventional ELISA methods have limited HRP labeling on anti-IgG antibodies. When HRP@SPCs are linked to the detection antibodies through the biotin–SA system, more HRP can be involved in the reaction. A highly sensitive assay can be easily obtained by generating a large number of signal tags from the HRP@SPC to generate an amplified detection signal.

To evaluate the specificity of the developed method, we also tested eight common pathogenic bacteria in spiked milk samples. A significantly increased optical density value in the *E. coli* O157:H7-spiked milk sample is shown in Figure 4C, whereas only minor changes were observed in all other samples, indicating excellent selectivity for *E. coli* O157:H7 determination. Recovery and coefficient of variation studies of *E. coli* O157:H7-spiked samples were conducted to evaluate the accuracy and precision of the proposed method. The results in Tables S2 and S3 indicate that our established HRP@SPC-based ELISA has high accuracy and precision and, therefore, could be used for practical applications.

#### 4. CONCLUSIONS

In this work, we used SPCs to encapsulate HRP or GOx to test the influence of nanoscale SPC encapsulation on the catalytic kinetics of HRP and GOx. The results indicate that the encapsulation can impact  $K_m$  and  $V_{max}$  of encapsulated enzymes as well as significantly amplify the enzymes' catalytic signals. We then tested the protection ability of 500 nm SPCs for encapsulated HRP in harsh pH, NaCl, and trypsin conditions as well as the storage stability. The stability study of HRP@SPCs and soluble HRP proved that SPCs could provide protection to packed enzymes in harsh conditions and increase the storage capability of HRP. GOx- and HRP-co-loaded SPCs also exhibited superiority for cascade catalysis in biosamples. The ability of SPCs to enhance enzyme-based immunoassays was tested by establishing a HRP@SPC-based ELISA to detect *E. coli* O157:H7. SPC-based ELISA exhibited an approximately 280-fold improvement in detection sensi-

tivity as compared with conventional ELISA. In summary, this work provides a systemic evaluation of 500 nm SPCs for enzyme immobilization and enhancing the detection performance of immunoassays.

#### ■ ASSOCIATED CONTENT

##### Supporting Information

The Supporting Information is available free of charge at <https://pubs.acs.org/doi/10.1021/acsomega.3c00180>.

Optimization of the number of double-layers for the coating of  $\text{CaCO}_3$  NPs; loading ability of  $\text{CaCO}_3$  NPs with HRP; photographs of HRP, HRP@ $\text{CaCO}_3$  NP-, SPC-, and HRP@SPC-catalyzed  $\text{H}_2\text{O}_2$  and TMB solutions; optimization of the catalytic conditions of soluble HRP and HRP@SPCs; steady-state kinetic assays of HRP and HRP@SPCs; steady-state kinetic assays of GOx and GOx@SPCs; laser scanning confocal microscopy images; effects of pH, temperature, concentration of glucose, and catalytic time on the catalytic ability; optimization of the labeling conditions of pH and the content of SA; checkerboard method for the concentration optimization of biotin@mAb and pAb; and recoveries of *E. coli* O157:H7 spiked into milk detected by HRP@SPC-based ELISA (PDF)

#### ■ AUTHOR INFORMATION

##### Corresponding Author

Yu Ding – Department of Food Science and Engineering, Institute of Food Safety and Nutrition, College of Science & Engineering, College of Life Science and Technology, Jinan University, Guangzhou 510632, China; [orcid.org/0000-0002-3688-7294](https://orcid.org/0000-0002-3688-7294); Email: [dingyu@jnu.edu.cn](mailto:dingyu@jnu.edu.cn)

##### Authors

Yanna Shao – Department of Food Science and Engineering, Institute of Food Safety and Nutrition, College of Science & Engineering, College of Life Science and Technology, Jinan University, Guangzhou 510632, China; Institute of Microbiology; State Key Laboratory of Applied Microbiology Southern China; Key Laboratory of Agricultural Microbiomics and Precision Application, Ministry of Agriculture and Rural Affairs; Guangdong Provincial Key Laboratory of Microbial Safety and Health, Guangdong Academy of Sciences, Guangzhou 510070, China

Yaofeng Zhou – Center for Hybrid Nanostructures (CHyN), Universität Hamburg, 22607 Hamburg, Germany; State Key Laboratory of Food Science and Technology, School of Food Science and Technology, Nanchang University, Nanchang 330047, China

Nuo Chen – Department of Food Science and Engineering, Institute of Food Safety and Nutrition, College of Science & Engineering, College of Life Science and Technology, Jinan University, Guangzhou 510632, China; Institute of Microbiology; State Key Laboratory of Applied Microbiology Southern China; Key Laboratory of Agricultural Microbiomics and Precision Application, Ministry of Agriculture and Rural Affairs; Guangdong Provincial Key Laboratory of Microbial Safety and Health, Guangdong Academy of Sciences, Guangzhou 510070, China

Wenxing Xu – Department of Food Science and Engineering, Institute of Food Safety and Nutrition, College of Science & Engineering, College of Life Science and Technology, Jinan

University, Guangzhou 510632, China; Institute of Microbiology; State Key Laboratory of Applied Microbiology Southern China; Key Laboratory of Agricultural Microbiomics and Precision Application, Ministry of Agriculture and Rural Affairs; Guangdong Provincial Key Laboratory of Microbial Safety and Health, Guangdong Academy of Sciences, Guangzhou 510070, China

**Huan Zhou** – Department of Food Science and Engineering, Institute of Food Safety and Nutrition, College of Science & Engineering, College of Life Science and Technology, Jinan University, Guangzhou 510632, China; Institute of Microbiology; State Key Laboratory of Applied Microbiology Southern China; Key Laboratory of Agricultural Microbiomics and Precision Application, Ministry of Agriculture and Rural Affairs; Guangdong Provincial Key Laboratory of Microbial Safety and Health, Guangdong Academy of Sciences, Guangzhou 510070, China

**Weihua Lai** – State Key Laboratory of Food Science and Technology, School of Food Science and Technology, Nanchang University, Nanchang 330047, China; [orcid.org/0000-0002-9305-1522](https://orcid.org/0000-0002-9305-1522)

**Xiaolin Huang** – State Key Laboratory of Food Science and Technology, School of Food Science and Technology, Nanchang University, Nanchang 330047, China

**Xinran Xiang** – Institute of Microbiology; State Key Laboratory of Applied Microbiology Southern China; Key Laboratory of Agricultural Microbiomics and Precision Application, Ministry of Agriculture and Rural Affairs; Guangdong Provincial Key Laboratory of Microbial Safety and Health, Guangdong Academy of Sciences, Guangzhou 510070, China

**Qinghua Ye** – Institute of Microbiology; State Key Laboratory of Applied Microbiology Southern China; Key Laboratory of Agricultural Microbiomics and Precision Application, Ministry of Agriculture and Rural Affairs; Guangdong Provincial Key Laboratory of Microbial Safety and Health, Guangdong Academy of Sciences, Guangzhou 510070, China

**Jumei Zhang** – Institute of Microbiology; State Key Laboratory of Applied Microbiology Southern China; Key Laboratory of Agricultural Microbiomics and Precision Application, Ministry of Agriculture and Rural Affairs; Guangdong Provincial Key Laboratory of Microbial Safety and Health, Guangdong Academy of Sciences, Guangzhou 510070, China

**Juan Wang** – College of Food Science, South China Agricultural University, Guangzhou 510432, China

**Wolfgang J. Parak** – Center for Hybrid Nanostructures (CHyN), Universität Hamburg, 22607 Hamburg, Germany; [orcid.org/0000-0003-1672-6650](https://orcid.org/0000-0003-1672-6650)

**Qingping Wu** – Institute of Microbiology; State Key Laboratory of Applied Microbiology Southern China; Key Laboratory of Agricultural Microbiomics and Precision Application, Ministry of Agriculture and Rural Affairs; Guangdong Provincial Key Laboratory of Microbial Safety and Health, Guangdong Academy of Sciences, Guangzhou 510070, China; [orcid.org/0000-0001-6503-359X](https://orcid.org/0000-0001-6503-359X)

Complete contact information is available at: <https://pubs.acs.org/10.1021/acsomega.3c00180>

### Author Contributions

Y.S. and Y.Z. contributed equally to this work. Y.S., Y.Z., and Y.D. conceived the project and designed the experiments; Y.S.,

Y.Z., N.C., W.X., H.Z., W.L., X.H., and X.X. performed the experiments; Y.S., Y.Z., N.C., W.X., H.Z., W.L., X.H., X.X., Q.Y., J.Z., J.W., W.J.P., Q.W., and Y.D. analyzed the data; Y.S., Y.Z., W.J.P., and Y.D. wrote the manuscript with assistance from the other authors.

### Notes

The authors declare no competing financial interest.

### ACKNOWLEDGMENTS

Y.D. and Q.W. were supported by the National Key R&D Program of China (2022YFF1100700), Guangdong Major Project of Basic and Applied Basic Research (2020B0301030005), Guangdong Provincial Key Laboratory (2020B121201009), and GDAS' Special Project of Science and Technology Development (2020GDASYL-20200103024). W.J.P. was supported by the Deutsche Forschungsgemeinschaft (DFG grant PA 794/21-2). Y.Z. is grateful for a PhD scholarship from the Chinese Scholarship Council.

### REFERENCES

- (1) Wu, Y.; Sun, J.; Huang, X.; Lai, W.; Xiong, Y. Ensuring food safety using fluorescent nanoparticles-based immunochromatographic test strips. *Trends Food Sci. Technol.* **2021**, *118*, 658–678.
- (2) Shao, Y.; Duan, H.; Zhou, S.; Ma, T.; Guo, L.; Huang, X.; Xiong, Y. Biotin–streptavidin system-mediated ratiometric multiplex immunochromatographic assay for simultaneous and accurate quantification of three mycotoxins. *J. Agric. Food Chem.* **2019**, *67*, 9022–9031.
- (3) Shao, Y.; Zhou, H.; Wu, Q.; Xiong, Y.; Wang, J.; Ding, Y. Recent advances in enzyme-enhanced immunosensors. *Biotechnol. Adv.* **2021**, *53*, 107867.
- (4) Zhou, Y.; Huang, X.; Zhang, W.; Ji, Y.; Chen, R.; Xiong, Y. Multi-branched gold nanoflower-embedded iron porphyrin for colorimetric immunosensor. *Biosens. Bioelectron.* **2018**, *102*, 9–16.
- (5) Zhou, Y.; Huang, X.; Xiong, S.; Li, X.; Zhan, S.; Zeng, L.; Xiong, Y. Dual-mode fluorescent and colorimetric immunoassay for the ultrasensitive detection of alpha-fetoprotein in serum samples. *Anal. Chim. Acta* **2018**, *1038*, 112–119.
- (6) Wang, Y.; Lu, M.; Tang, D. Novel photoluminescence enzyme immunoassay based on supramolecular host-guest recognition using L-arginine/6-aza-2-thiothymine-stabilized gold nanocluster. *Biosens. Bioelectron.* **2018**, *109*, 70–74.
- (7) Yang, N.; Huang, Y.; Ding, G.; Fan, A. In situ generation of prussian blue with potassium ferrocyanide to improve the sensitivity of chemiluminescence immunoassay using magnetic nanoparticles as label. *Anal. Chem.* **2019**, *91*, 4906–4912.
- (8) Xiong, Y.; Leng, Y.; Li, X.; Huang, X.; Xiong, Y. Emerging strategies to enhance the sensitivity of competitive ELISA for detection of chemical contaminants in food samples. *Trends Anal. Chem.* **2020**, *126*, 115861.
- (9) Yan, X.; Wang, T.; Yao, D.; Xu, J.; Luo, Q.; Liu, J. Interfacial assembly of signal amplified multienzymes and biorecognized antibody into proteinosome for an ultrasensitive immunoassay. *Small* **2019**, *15*, 1900350.
- (10) Huang, J.; Jiao, L.; Xu, W.; Fang, Q.; Wang, H.; Cai, X.; Yan, H.; Gu, W.; Zhu, C. Immobilizing enzymes on noble metal hydrogel nanozymes with synergistically enhanced peroxidase activity for ultrasensitive immunoassays by cascade signal amplification. *ACS Appl. Mater. Interfaces* **2021**, *13*, 33383–33391.
- (11) Wang, X.; Wang, H.; Tang, J.; Wang, S.; Shi, D.; Shen, H. Poly (amino acid) multilayers modified dendritic mesoporous silica nanoparticles achieve effective enzyme stability for ultrasensitive immunoassay. *ACS Appl. Mater. Interfaces* **2020**, *12*, 37906–37913.
- (12) Hsu, M. N.; Wei, S. C.; Phan, D. T.; Zhang, Y.; Chen, C. H. Nano-in-micro smart hydrogel composite for a rapid sensitive immunoassay. *Adv. Healthcare Mater.* **2019**, *8*, 1801277.

- (13) Pan, Y.; Li, H.; Farmakes, J.; Xiao, F.; Chen, B.; Ma, S.; Yang, Z. How do enzymes orient when trapped on metal–organic framework (MOF) surfaces? *J. Am. Chem. Soc.* **2018**, *140*, 16032–16036.
- (14) Tran, D. N.; Balkus, K. J., Jr. Perspective of recent progress in immobilization of enzymes. *ACS Catal.* **2011**, *1*, 956–968.
- (15) Weltz, J. S.; Kienle, D. F.; Schwartz, D. K.; Kaar, J. L. Dramatic increase in catalytic performance of immobilized lipases by their stabilization on polymer brush supports. *ACS Catal.* **2019**, *9*, 4992–5001.
- (16) Mahmoud, K. A.; Male, K. B.; Hrapovic, S.; Luong, J. H. Cellulose nanocrystal/gold nanoparticle composite as a matrix for enzyme immobilization. *ACS Appl. Mater. Interfaces* **2009**, *1*, 1383–1386.
- (17) Wu, L.; Li, G.; Xu, X.; Zhu, L.; Huang, R.; Chen, X. Application of nano-ELISA in food analysis: recent advances and challenges. *Trends Anal. Chem.* **2019**, *113*, 140–156.
- (18) Neupane, S.; Patnode, K.; Li, H.; Baryeh, K.; Liu, G.; Hu, J.; Chen, B.; Pan, Y.; Yang, Z. Enhancing enzyme immobilization on carbon nanotubes via metal–organic frameworks for large-substrate biocatalysis. *ACS Appl. Mater. Interfaces* **2019**, *11*, 12133–12141.
- (19) Llopis-Lorente, A.; García-Fernández, A.; Murillo-Cremaes, N.; Hortelão, A. C.; Patiño, T.; Villalonga, R.; Sancenón, F.; Martínez-Mañez, R.; Sánchez, S. Enzyme-powered gated mesoporous silica nanomotors for on-command intracellular payload delivery. *ACS Nano* **2019**, *13*, 12171–12183.
- (20) Chiang, C.-W.; Liu, X.; Sun, J.; Guo, J.; Tao, L.; Gao, W. Polymerization-induced coassembly of enzyme–polymer conjugates into comicelles with tunable and enhanced cascade activity. *Nano Lett.* **2019**, *20*, 1383–1387.
- (21) Ganaja, K. A.; Chaplan, C. A.; Zhang, J.; Martinez, N. W.; Martinez, A. W. Paper microzone plates as analytical tools for studying enzyme stability: a case study on the stabilization of horseradish peroxidase using trehalose and SU-8 epoxy novolac resin. *Anal. Chem.* **2017**, *89*, 5333–5341.
- (22) Li, M.; Qiao, S.; Zheng, Y.; Andaloussi, Y. H.; Li, X.; Zhang, Z.; Li, A.; Cheng, P.; Ma, S.; Chen, Y. Fabricating covalent organic framework capsules with commodious microenvironment for enzymes. *J. Am. Chem. Soc.* **2020**, *142*, 6675–6681.
- (23) Chen, S.-Y.; Lo, W.-S.; Huang, Y.-D.; Si, X.; Liao, F.-S.; Lin, S.-W.; Williams, B. P.; Sun, T.-Q.; Lin, H.-W.; An, Y.; Sun, T.; Ma, Y.; Yang, H.-C.; Chou, L.-Y.; Shieh, F.-K.; Tsung, C.-K. Probing interactions between metal–organic frameworks and freestanding enzymes in a hollow structure. *Nano Lett.* **2020**, *20*, 6630–6635.
- (24) Weltz, J. S.; Kienle, D. F.; Schwartz, D. K.; Kaar, J. L. Reduced enzyme dynamics upon multipoint covalent immobilization leads to stability-activity trade-off. *J. Am. Chem. Soc.* **2020**, *142*, 3463–3471.
- (25) Sun, Q.; Fu, C.-W.; Aguila, B.; Perman, J.; Wang, S.; Huang, H.-Y.; Xiao, F.-S.; Ma, S. Pore environment control and enhanced performance of enzymes infiltrated in covalent organic frameworks. *J. Am. Chem. Soc.* **2018**, *140*, 984–992.
- (26) Zou, X.; Wei, S.; Badiyan, S.; Schroeder, M.; Jasensky, J.; Brooks, C. L., III; Marsh, E. N. G.; Chen, Z. Investigating the effect of two-point surface attachment on enzyme stability and activity. *J. Am. Chem. Soc.* **2018**, *140*, 16560–16569.
- (27) Roy, S.; Zhu, D.; Parak, W. J.; Feliu, N. Lysosomal proton buffering of poly (ethylenimine) measured in situ by fluorescent pH-sensor microcapsules. *ACS Nano* **2020**, *14*, 8012–8023.
- (28) Kanungo, S.; Paunovic, V.; Schouten, J. C.; Neira D'Angelo, M. F. Facile synthesis of catalytic AuPd nanoparticles within capillary microreactors using polyelectrolyte multilayers for the direct synthesis of H<sub>2</sub>O<sub>2</sub>. *Nano Lett.* **2017**, *17*, 6481–6486.
- (29) Gao, C.; Liu, X.; Shen, J.; Möhwald, H. Spontaneous deposition of horseradish peroxidase into polyelectrolyte multilayer capsules to improve its activity and stability. *Chem. Commun.* **2002**, 1928–1929.
- (30) Becker, A. L.; Johnston, A. P.; Caruso, F. Layer-by-layer-assembled capsules and films for therapeutic delivery. *Small* **2010**, *6*, 1836–1852.
- (31) Caruso, F.; Trau, D.; Möhwald, H.; Renneberg, R. Enzyme encapsulation in layer-by-layer engineered polymer multilayer capsules. *Langmuir* **2000**, *16*, 1485–1488.
- (32) Nazareus, M.; Abasolo, I.; García-Aranda, N.; Voccoli, V.; Rejman, J.; Cecchini, M.; Schwartz, S., Jr.; RiveraGil, P.; Parak, W. J. Polymer capsules as a theranostic tool for a universal in vitro screening assay—the case of lysosomal storage diseases. *Part. Part. Syst. Charact.* **2015**, *32*, 991–998.
- (33) Ochs, M.; Carregal-Romero, S.; Rejman, J.; Braeckmans, K.; De Smedt, S. C.; Parak, W. J. Light-addressable capsules as caged compound matrix for controlled triggering of cytosolic reactions. *Angew. Chem., Int. Ed.* **2013**, *52*, 695–699.
- (34) Harimech, P. K.; Hartmann, R.; Rejman, J.; del Pino, P.; Rivera-Gil, P.; Parak, W. J. Encapsulated enzymes with integrated fluorescence-control of enzymatic activity. *J. Mater. Chem. B* **2015**, *3*, 2801–2807.
- (35) Jin, W.; Shi, X.; Caruso, F. High activity enzyme microcrystal multilayer films. *J. Am. Chem. Soc.* **2001**, *123*, 8121–8122.
- (36) Shchukin, D. G.; Shutava, T.; Shchukina, E.; Sukhorukov, G. B.; Lvov, Y. M. Modified polyelectrolyte microcapsules as smart defense systems. *Chem. Mater.* **2004**, *16*, 3446–3451.
- (37) Oaew, S.; Charlermroj, R.; Pattarakankul, T.; Karoonuthaisiri, N. Gold nanoparticles/horseradish peroxidase encapsulated polyelectrolyte nanocapsule for signal amplification in *Listeria monocytogenes* detection. *Biosens. Bioelectron.* **2012**, *34*, 238–243.
- (38) Yu, X.; Li, Y.; Liu, X.; Qiao, B.; Yang, Y.; Zhang, Y.; Hu, P.; Lu, S.; Ren, H.; Liu, Z.; Liu, M.; Zhou, Y. Polyelectrolyte nanocapsule probe for the determination of imidacloprid in agricultural food samples. *Food Agric. Immunol.* **2019**, *30*, 432–445.
- (39) Dong, Z.; Feng, L.; Hao, Y.; Li, Q.; Chen, M.; Yang, Z.; Zhao, H.; Liu, Z. Synthesis of CaCO<sub>3</sub>-based nanomedicine for enhanced sonodynamic therapy via amplification of tumor oxidative stress. *Chem* **2020**, *6*, 1391–1407.
- (40) Gao, H.; Goriacheva, O. A.; Tarakina, N. V.; Sukhorukov, G. B. Intracellularly biodegradable polyelectrolyte/silica composite microcapsules as carriers for small molecules. *ACS Appl. Mater. Interfaces* **2016**, *8*, 9651–9661.
- (41) Chen, G.; Kou, X.; Huang, S.; Tong, L.; Shen, Y.; Zhu, W.; Zhu, F.; Ouyang, G. Modulating the biofunctionality of metal–organic-framework-encapsulated enzymes through controllable embedding patterns. *Angew. Chem., Int. Ed.* **2020**, *59*, 2867–2874.
- (42) Liu, L.; Shi, Y.; Yang, Y.; Li, M.; Long, Y.; Huang, Y.; Zheng, H. Fluorescein as an artificial enzyme to mimic peroxidase. *Chem. Commun.* **2016**, *52*, 13912–13915.
- (43) Zhang, Y.; Tsitkov, S.; Hess, H. Proximity does not contribute to activity enhancement in the glucose oxidase–horseradish peroxidase cascade. *Nat. Commun.* **2016**, *7*, 13982.
- (44) Shao, Y.; Duan, H.; Guo, L.; Leng, Y.; Lai, W.; Xiong, Y. Quantum dot nanobead-based multiplexed immunochromatographic assay for simultaneous detection of aflatoxin B1 and zearalenone. *Anal. Chim. Acta* **2018**, *1025*, 163–171.
- (45) Gregurec, D.; Olszyna, M.; Politakos, N.; Yate, L.; Dahne, L.; Moya, S. E. Stability of polyelectrolyte multilayers in oxidizing media: A critical issue for the development of multilayer based membranes for nanofiltration. *Colloid Polym. Sci.* **2015**, *293*, 381–388.
- (46) Caruso, F.; Schüler, C. Enzyme multilayers on colloid particles: assembly, stability, and enzymatic activity. *Langmuir* **2000**, *16*, 9595–9603.
- (47) Tsitkov, S.; Hess, H. Design principles for a compartmentalized enzyme cascade reaction. *ACS Catal.* **2019**, *9*, 2432–2439.
- (48) Chen, Y.; Yuan, M.; Zhang, Y.; Liu, S.; Yang, X.; Wang, K.; Liu, J. Construction of coacervate-in-coacervate multi-compartment protocells for spatial organization of enzymatic reactions. *Chem. Sci.* **2020**, *11*, 8617–8625.
- (49) Qin, X.; Wu, C.; Niu, D.; Qin, L.; Wang, X.; Wang, Q.; Li, Y. Peroxisome inspired hybrid enzyme nanogels for chemodynamic and photodynamic therapy. *Nat. Commun.* **2021**, *12*, 5243.

(50) Wu, Y.; Zhou, Y.; Leng, Y.; Lai, W.; Huang, X.; Xiong, Y. Emerging design strategies for constructing multiplex lateral flow test strip sensors. *Biosens. Bioelectron.* **2020**, *157*, 112168.

(51) Fu, J.; Zhou, Y.; Huang, X.; Zhang, W.; Wu, Y.; Fang, H.; Zhang, C.; Xiong, Y. Dramatically enhanced immunochromatographic assay using cascade signal amplification for ultrasensitive detection of *Escherichia coli* O157: H7 in milk. *J. Agric. Food Chem.* **2020**, *68*, 1118–1125.